Science Bulletin 64 (2019) 1700–1706

Contents lists available at ScienceDirect

Science Bulletin

journal homepage: www.elsevier.com/locate/scib

Science Bulletin
www.scibull.com

Article

Efficient passivation of monolayer MoS_2 by epitaxially grown 2D organic crystals

Xin Xu [a], Zefeng Chen [a], Beilei Sun [a], Yu Zhao [a,b], Li Tao [a,*], Jian-Bin Xu [a,*]

[a] Department of Electronic Engineering, The Chinese University of Hong Kong, Hong Kong, China
[b] Guangdong Provincial Key Laboratory of Functional Soft Condensed Matter, School of Material and Energy, Guangdong University of Technology, Guangzhou 510006, China

ARTICLE INFO

Article history:
Received 25 June 2019
Received in revised form 20 August 2019
Accepted 4 September 2019
Available online 9 September 2019

Keywords:
Molybdenum disulfide
Filed-effect transistor
Photodetector
Passivation

ABSTRACT

Monolayer molybdenum disulfide (MoS_2) is considered to be a promising candidate for field-effect transistors and photodetectors due to its direct bandgap and atomically thin properties. However, the MoS_2 devices are impeded by the intrinsic surface defects and environmental adsorption such as H_2O and O_2. Here, we demonstrated a highly ordered, ultrathin (<5 nm) and scalable *N*,*N*′-ditridecylperylene-3,4,9,10-tetracarboxylic diimide (PTCDI-C13) passivation layer that can be epitaxially grown on MoS_2. The van der Waals interface between PTCDI-C13 and MoS_2 can efficiently reduce the surface traps and isolate MoS_2 from ambient. As a result, the passivated devices exhibit huge improvement in both carrier mobility (from 0.5 to 8.3 $cm^2/(V\,s)$) and sub-threshold swing (from 16.7 to 1.6 V/dec). Also, the photodetector made on MoS_2 after passivation has a much faster response speed (from 3 s to 10 ms) without significant sacrifice of the responsivity. Our method provides a facile approach to realize high-performance two-dimensional electronic and optoelectronic devices.

1. Introduction

Two-dimensional transition metal dichalcogenides (2D TMDs) have attracted extensive attention in recent years [1–3]. Due to the unique properties of thickness-dependent band structure and atomically-thin nature which provides a gate-tunable transport behavior, they are supposed to be powerful candidates of the next-generation low-power nano-electronic devices. As one of the most representative TMDs, large-area MoS_2 has been successfully fabricated by various methods, particularly chemical vapor deposition (CVD) [4,5]. Many kinds of devices such as photodetectors6 [7], and field-effect transistors (FETs) [8,9] based on MoS_2 were studied and showed a broad application prospect in the field of optoelectronics.

However, the existence of intrinsic defects which result from the deficiency of sulfur atom on the surface of MoS_2 severely limits the application of MoS_2 based devices [10–13]. The substantial density of deep trapping states for carriers and photogating effect renders a large hysteresis in FETs and slow response dynamics and persistent photoconductance in photodetectors [6,14–16]. Also, due to the atomically-thin nature, the surface absorbents of O_2 and H_2O can largely disturb the carrier transport in the channel and lead to the instability issue in ambient [7,17,18]. As a result, the carrier mobility is significantly decreased and the sub-threshold slope (*SS*) becomes very large in a long-term durability experiment.

Surface passivation with capping layers is an effective strategy to deal with these problems in 2D materials [19–22]. One idea is to encapsulate 2D materials with Al_2O_3 [23,24], HfO_2 [7,8], or hexagonal boron nitride (hBN) [25–27] which can isolate MoS_2 from the air to improve the performances of the FET devices. However, due to the lack of surface dangling bonds of MoS_2, the atomic layer deposition (ALD)-processed oxide capping layers show non-uniform growth and can hardly realize full coverage when the protective layer is ultra-thin [18], and serious n-type doping commonly occurs due to the ALD process [7]. Encapsulation with exfoliated hBN involves exquisite manipulations and is not practically suitable for scalable processing. Alternatively, organic molecules (especially the phthalocyanine and its metal derivatives) were used to be assembled on the surface of TMDs by both solution-process and vapor-phase methods which enable passivation of the surface defects [12,28–33]. Furthermore, these passivation can modulate the response speed of the photodetector by taking advantage of the van der Waals (vdW) interface between the organic molecule and MoS_2 [28,29]. However, the protective molecules can hardly achieve atomic uniformity on MoS_2, and the thickness is uncontrollable up to now, which hampers the

* Corresponding authors.
E-mail addresses: litao@cuhk.edu.hk (L. Tao), jbxu@ee.cuhk.edu.hk (J.-B. Xu).

https://doi.org/10.1016/j.scib.2019.09.009
2095-9273/

protection ability [34]. Additionally, albeit the passivation increases the response speed, the photocurrent decreases dramatically with several orders of magnitude [28,29,35].

Here, we develop a highly efficient passivation technique for monolayer MoS_2 with epitaxially grown atomically-thin organic crystalline film of *N*,*N*′-ditridecylperylene-3,4,9,10-tetracarboxylic diimide (PTCDI-C13). The PTCDI-C13 molecules are assembled on the MoS_2 surface with high order, forming a vdW interface that can fully encapsulate the MoS_2 surface with a single uniform layer [36]. In comparison with the control devices, we find that the mobility of passivated MoS_2 devices increases by one order of magnitude and the *SS* decreases by one order of magnitude. In addition, the passivation highly improves the photoresponse dynamics of MoS_2. The response speed increases by three orders of magnitude due to the removal of deep trapping states. The long-term stability of the MoS_2 devices also proves to be significantly enhanced with the 2D organic crystal passivation. Our results suggest that the self-assembled atomically-thin organic crystal can significantly passivate the defective MoS_2 surface, rendering the largely enhanced performance of MoS_2 devices.

2. Experimental

2.1. Crystal growth

Monolayer MoS_2 films were grown by CVD method in a 2-inch quartz tube under 100 Pa with 10 sccm H_2 and 100 sccm Ar. The growth substrate is p++ silicon with 300 nm SiO_2 on the top surface. The growth temperature is around 800 °C and the growth time is about 15 min. The ultra-thin PTCDI-C13 films were grown on MoS_2 surface by physical vapor transport (PVT) method in a 1-inch quartz tube under high vacuum ($\sim 10^{-4}$ Pa) with PTCDI-C13 powder (95%) as the source material. The distance between source and growth substrate is around 19 cm. The source was heated to 220–240 °C for the PVT process and the growth time was ~90 min.

2.2. Characterization

The atomic force microscopy (AFM) images were taken using Bruker Dimension Icon in air. Raman/photoluminescence (PL) measurements were performed with HORIBA LabRAM HR Evolution system with 532 nm laser excitation at room temperature. The laser power was set at 0.1 mW and the size of the laser spot was ~1 μm. The selected area electron diffraction (SAED) experiments were conducted using Tecnai T12 TEM system.

2.3. Device fabrication

The 100 nm thick gold films were transferred onto the top of MoS_2 as source and drain electrodes by tungsten tips under a microscope. The p++ silicon was used as a global back gate. For the passivated devices, PTCDI-C13 molecules were grown onto the surface by PVT method before transferring the electrodes.

2.4. Device measurements

Electrical measurements were performed by Keithley 4200 semiconductor parameter analyzer. A 532 nm laser was applied for the measurements of steady photocurrent. For the dynamic photoresponse experiments, all the measurements were conducted under the condition of gate voltage $V_g = 0$ V and bias voltage $V_{ds} = 1$ V. The laser's wavelength is 650 nm (powder density of 1 mW/cm^2).

3. Results and discussion

Monolayer MoS_2 was synthesized by CVD method on SiO_2/Si substrate as previously reported [5,37]. The monolayer (1L) PTCDI-C13 molecules are epitaxially grown on the MoS_2 layer by PVT method, with details available in the Experimental Section and Fig. S1 (online). Fig. 1a is the optical image of the large triangular domains of monolayer MoS_2. The height information of both monolayer MoS_2 and 1L PTCDI-C13 on MoS_2 is obtained by AFM as shown in Fig. 1b, e. The thickness of monolayer MoS_2 is ~1 nm and the height of 1L PTCDI-C13 is ~2.6 nm [38]. Note that between the monolayer MoS_2 and 1L PTCDI-C13, there exists another layer of PTCDI-C13 on the surface of MoS_2, which is called the interfacial layer (IL) [39]. Due to the stronger interaction between MoS_2 and IL PTCDI-C13, the IL molecules are lying down on MoS_2, causing a smaller thickness (~0.9 nm) than the 1L (~2.6 nm) (Fig. S2 online). In comparison with other passivation methods, our passivation method possesses much more uniform surface morphology with the root mean square average (RMS) roughness of 0.3 nm (1.3 nm for the MoS_2 passivated with Al_2O_3) [40]. The coverage of the grown PTCDI-C13 on MoS_2 is determined by the distance between source (PTCDI-C13 powder) and substrate (SiO_2) and growth time during the PVT process. With the optimized growth parameters (see Experiment Section), we obtain the full coverage of 1L PTCDI-C13 on MoS_2 (evidenced by Raman intensity map in Fig. S3 (online)). Benefited from both the atomic-scale flatness and full coverage of PTCDI-C13, both the electrical performance and optoelectronic properties of MoS_2 devices passivated by our method are able to be greatly boosted, as we will discuss later in detail.

PL spectrum reveals the exciton energy of a material which is another important way to study the material properties. We have compared the PL spectra before and after passivation as shown in Fig. 1c. The PL spectrum of monolayer MoS_2 has a peak around 672 nm as the black line indicates, corresponding to the monolayer MoS_2's direct bandgap near 1.8 eV [41]. After the growth of PTCDI-C13, two additional PL peaks appear at 621 and 673 nm, resulting from the interaction between PTCDI-C13 layers [42]. Raman spectra for MoS_2 before and after passivation are also compared as shown in Fig. 1f. The two characteristic peaks of monolayer MoS_2 (E^1_{2g} at 384 cm^{-1} and A_{1g} at 404 cm^{-1}) remain unchanged while four new peaks appear after the deposition of PTCDI-C13, corresponding to the Raman signal of PTCDI-C13 molecules. Two peaks at 1295 and 1374 cm^{-1} correspond to carbon-hydrogen (C—H) bond and the other two peaks at 1450 and 1568 cm^{-1} correspond to the benzene ring signal [43]. These Raman signals along with AFM images evidently corroborate the existence of PTCDI-C13 molecules on the MoS_2 surface. To probe the crystal properties of the grown PTCDI-C13, we have conducted the SAED experiments on the PTCDI-C13/MoS_2. As shown in Fig. S4 (online), the SAED pattern indicates the single crystalline nature of PTCDI-C13 grown on the MoS_2 triangular grain. Furthermore, we have randomly picked several points on the surface of PTCDI-C13 and checked the polarized PL spectra (Fig. S5 online). It turns out that all the points in the same MoS_2 triangular grain exhibit identical anisotropy direction with no more than 2° in error. This further proves that the PTCDI-C13 molecules are epitaxially grown on MoS_2.

To explore the electrical properties of MoS_2 both before and after PTCDI-C13 deposition, a bottom-gate top-contact device configuration is adopted as depicted in Fig. 2e. The step-by-step fabrication process is shown in Fig. S6 (online). Note that the PTCDI-C13 itself is almost non-conductive in air, although a relatively high carrier mobility of 2.1 cm^2/(V s) under vacuum condition has been reported [44,45]. Hence, the PTCDI-C13 film grown on MoS_2 hardly contributes to the channel carrier transport in air. By comparing

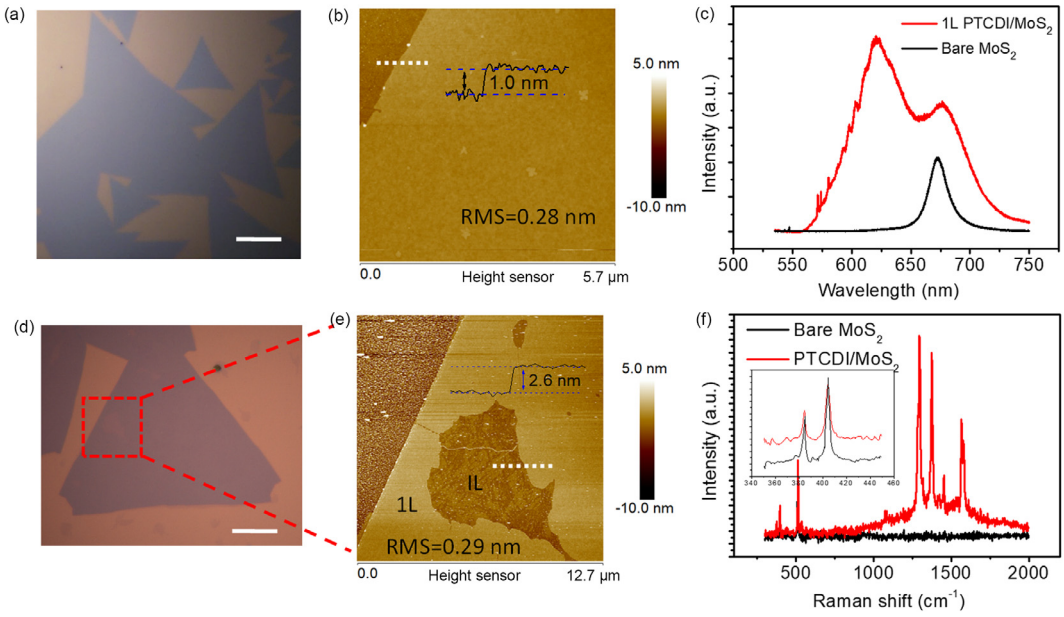

Fig. 1. (Color online) Optical images of monolayer MoS_2 prepared by CVD method (a) before and (d) after PTCDI-C13 deposition. Scale bars: 10 μm. (b), (e) AFM images of monolayer MoS_2 and PTCDI-C13 molecule on MoS_2. Insets show the height information of monolayer MoS_2 and 1L PTCDI-C13. (c) PL spectra of bare MoS_2 and 1L PTCDI-C13 on MoS_2. (f) Raman spectra of bare MoS_2 and MoS_2 with PTCDI-C13. Insets are details of the MoS_2 E^1_{2g} and A_{1g} peaks.

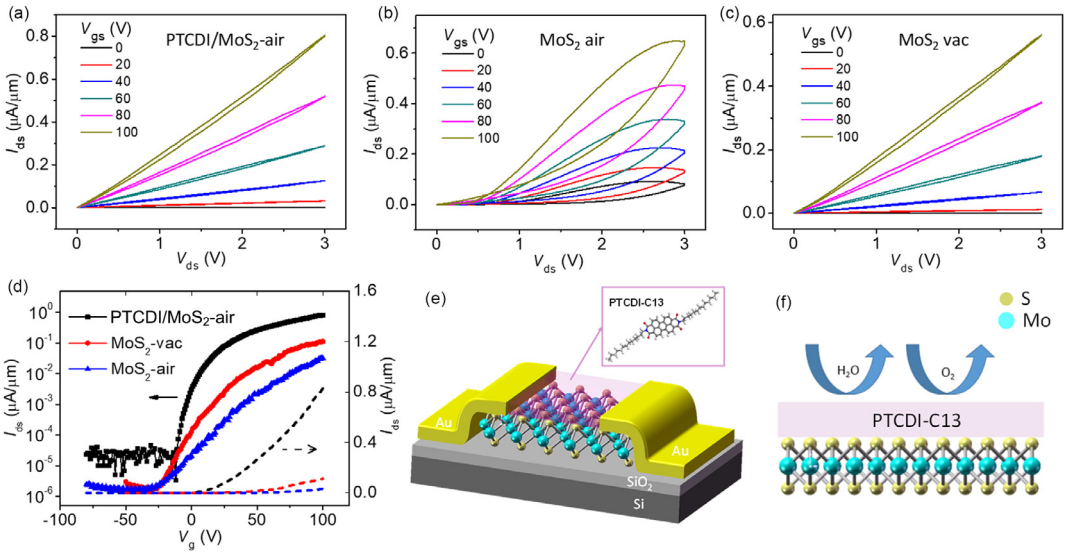

Fig. 2. (Color online) (a) The output curves of MoS_2 passivated by PTCDI-C13 tested under ambient conditions with different gate voltages. The output curves of bare MoS_2 tested under (b) ambient and (c) vacuum conditions. (d) The transfer characteristics of MoS_2 before and after PTCDI-C13 deposition (V_{ds} = 5 V). (e) A 3D sketch of the typical MoS_2 FET with passivation. (f) A 2D sketch that illustrates how passivation layer isolates MoS_2 layer from water and oxygen in air.

with the output characteristics (I_{ds}-V_{ds}) of the bare monolayer MoS_2 which has a memory window of ~1 V (Fig. 2b), we can easily find an obvious vanish of the hysteresis after the passivation by PTCDI-C13 (Fig. 2a). As previously reported, the huge hysteresis in bare MoS_2 devices is mainly due to the absorption of O_2 and H_2O in the air by vacancies of sulfur atoms [7,32,46]. To further confirm this conclusion, the same bare MoS_2 devices were tested under vacuum conditions which possibly eliminates the ambient effects on MoS_2 layer (Fig. 2c). We can see that the pristine devices in vacuum behave like the passivated ones and the I_{ds}-V_{ds} curves show a good linear relationship. On the basis of the above comparative investigation of the MoS_2 FET performance, it is demonstrated that the O_2 and H_2O molecules are effectively isolated from the MoS_2 surface by the PTCDI-C13 deposition as illustrated in Fig. 2f. Also, the linear I_{ds}-V_{ds} curves demonstrate that the passivation delivers better Ohmic contacts of the electrodes [26,47].

The transfer characteristics (I_{ds}-V_{gs}) of MoS_2 after passivation also obtained a huge improvement in several aspects (Fig. 2d). First, the sub-threshold slope $\left(SS = \frac{\partial V_{gs}}{\partial(\log I_{ds})}\right)$ reduces from 16.7 to 1.6 V/dec after the MoS_2 is passivated. Second, the field-effect carrier mobility extracted from the transfer curves performs a significant augment from 0.5 to 8.3 $cm^2/(V\,s)$. Also, we tested the bare MoS_2 device under vacuum conditions, and found that the *SS* and mobility (8.7 V/dec and 1.4 $cm^2/(V\,s)$, respectively) are improved in comparison with the same device measured in air, but still inferior to the passivated device in air. This indicates that the PTCDI-C13 molecule passivation not only effectively isolates the MoS_2

surface from the ambient, but also deactivates the intrinsic defects in MoS_2 (i.e., the sulfur vacancies), delivering the greatly enhanced electrical characteristics of the MoS_2 [12,28,29]. From the equation $SS = 2.3 \times \frac{k_B T}{q}\left(1 + \frac{q^2 D_{it}}{C_{ox}}\right)$, where k_B, T, q, D_{it} and C_{ox} are the Boltzmann constant, temperature, elementary charge, interface trap density and oxide capacitance (1.15×10^{-8} F/cm^2), respectively, we can estimate that the interface trap density in MoS_2 (D_{it}) decreases from 2.1×10^{13} to 1.8×10^{12} eV^{-1} cm^{-2} due to the passivation [48]. The threshold voltage (V_{th}) moves from 12 to −8 V after the molecular passivation. The hysteresis in transfer characteristic is highly reduced as well (Fig. S7 online), similar to the case of output curve hysteresis as we discussed precedingly. Statistical data of *SS* and mobility collected from several devices are plotted in Fig. S8 (online), which provides more details on the impact of passivation on the device performance.

Compared with other passivated devices that have the similar structures, our devices show an overall improvement. Both the *SS* and mobility are improved by one order of magnitude after passivation (Table 1). More importantly, the passivation layer is uniformly distributed with thickness of only 2.6 nm while the other methods usually adopt 30 nm or thicker protective layer. Also, our method can be carried out in a much simpler way for scalable fabrication. Besides MoS_2, we have tested monolayer WS_2 FET as well, whose performance is also improved after passivation as shown in Fig. S9 (online). The 2D organic film passivation method is believed to be applicable for other unstable 2D semiconducting materials such as black phosphorus and InSe.

To investigate the effects of PTCDI-C13 passivation on the long-term stability of the MoS_2 FET devices, two groups of monolayer MoS_2 devices were prepared with the same parameters and stored in the same ambient conditions. One group of the devices was passivated and the other one remains bare. The normalized mobility extracted from the representative MoS_2 devices with and without passivation as storage time increases are depicted in Fig. 3a. While the mobility of the device after passivation reserved ~71% of its initial value, the bare MoS_2 device loses most of its mobility (3.8% remained) after exposed to air for 10 d due to the degradation induced by dislocations and point defects in MoS_2 [49,50]. Fig. 3b, c shows the transfer characteristics measured after different air storing times with and without PTCDI-C13 passivation, respectively. An obvious degradation of on-current density can be found in the unprocessed devices, while the on-current retains the same order of magnitude in the passivated device.

Next, we focus on the optoelectronic characteristics of the MoS_2 devices before and after PTCDI-C13 passivation. The photoresponse measurements were conducted with a 532 nm laser in ambient. The transfer curves in the dark and under various illumination intensities are plotted in Fig. 4a, b. With the increase of laser power, the threshold voltages V_{th} of both devices move towards the negative direction and the on-currents increase by one or two orders of magnitude which are known as the photogating effect [14]. Compared with the devices without passivation, these devices after passivation have a much small movement of their threshold voltage, which means that the photogating effect is efficiently diminished by passivation. By introducing the PTCDI-C13 passivation layer, a majority of the deep defect states in the monolayer MoS_2 are removed. As a result, the defect-induced photogating effects are largely suppressed.

To gain deeper insights, the photo responsivity as a function of the power intensity was measured at several different gate voltages as plotted in Fig. 4c, d. A sketch of band alignments (Fig. 4e, f) is helpful to understand the physical picture behind this experiment [7,28,29]. For the deep traps, their recombination time is very long, which causes the large responsivity but slow response speed [28,51]. For the shallow traps, their recombination time is relatively short, delivering a small responsivity but fast response speed. First, we focus on the situation when V_g is near V_{th}, as indicated by the "0 V" and "−30 V" lines in Fig. 4c, d. In this case the Fermi level of MoS_2 is near the conduction band (Fig. 4e) and the excessive carriers can be seized by traps. For the passivated devices (Fig. 4c), as the deep trap states in the MoS_2 have been efficiently reduced, the shallow trap states are dominating until most of them are occupied with the increasing light intensity. As a result, the responsivity of the passivated device remains unchanged at about 150 A/W under small light power intensity and then decrease to 0.5 A/W under large power intensity when the shallow traps are all occupied. However, the responsivity of the devices without passivation shows a monotonic decrease with increasing the illumination power ("0 V" and "−30 V" lines in Fig. 4d). This mainly results from the deep trap states existed in the bare MoS_2 layers. With the increase of laser intensity, more deeper trap states are occupied and then the shallow traps are dominating, which renders the decrease of responsivity. The large responsivity change from 1029 to 3 A/W also proves that the dominant type of traps is

Table 1
Comparison of the device electrical attributes before/after passivation.

Device structure	*SS* (V/dec)	Mobility (cm^2/(V s))	On/off ratio	Passivation layer thickness (nm)	Ref.
PTCDI-C13/MoS_2 (epitaxial growth)	16.7/1.6	0.5/8.3	$5 \times 10^4/5 \times 10^4$	2.6	This work
TiOPc/MoS_2 (thermal deposition)	6.7/1.6	NA	$10^4/10^7$	NA	[12]
HfO_2/MoS_2 (ALD)	NA	0.5/12	$10^4/10^6$	30	[7]
PMMA/MoS_2 (coating)	NA	2.1/4.9	NA	260	[22]

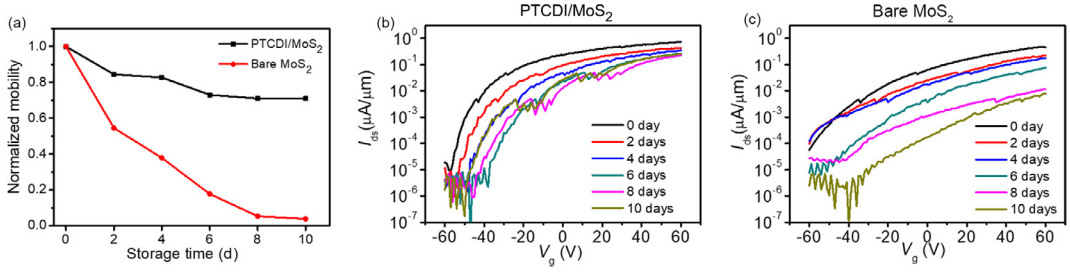

Fig. 3. (Color online) (a) Stability experiment about the mobility of MoS_2 FETs devices with and without passivation. All the devices are stored in air at room temperature and measured in air. (b) Transfer curves of MoS_2 passivated by PTCDI-C13. (c) Transfer curves of the bare MoS_2. All the devices are measured under bias voltage V_{ds} = 3 V.

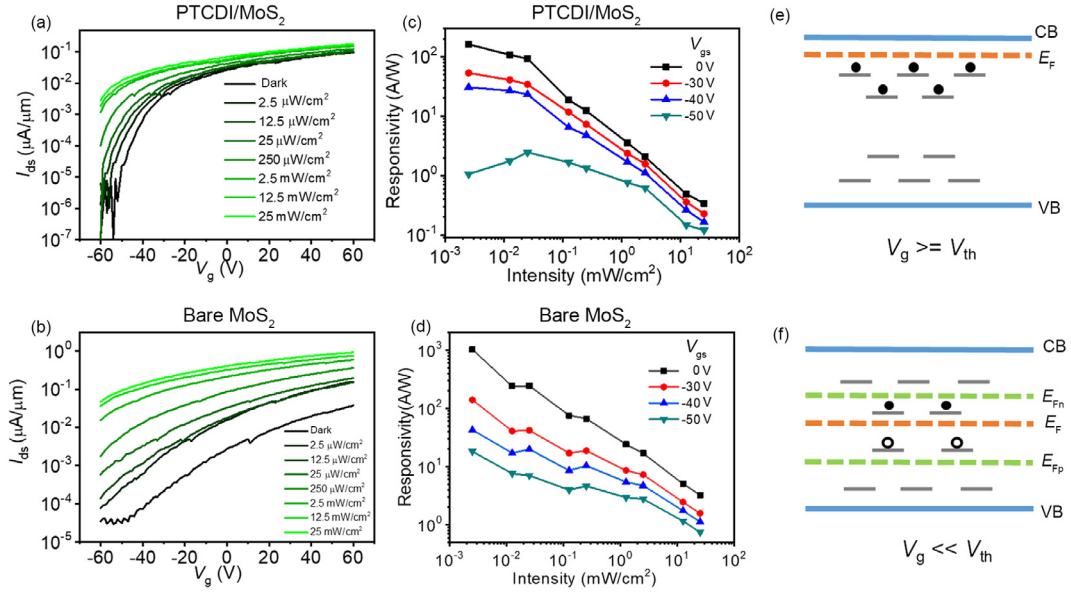

Fig. 4. (Color online) Transfer characteristics ($I_{ds} - V_{gs}$) of MoS_2 (a) with and (b) without passivation under 532 nm laser illumination with different intensities (from 25 to 2.5×10^{-3} mW/cm^2). (c), (d) Power-dependent responsivity under different gate voltages from 0 to −50 V of MoS_2 with and without passivation. Diagrams of band alignment showing carrier generation and trapping dynamics when (e) gate voltage V_g is near the threshold voltage V_{th}, and (f) V_g is much smaller than threshold voltage V_{th}.

changing from deep trap into shallow trap. And then we focus on the situation when V_g is much smaller than V_{th} ("−50 V" lines in Fig. 4c, d). In this case, the Fermi level is under the conduction band and there exist some unoccupied states between the conduction band and valance band (Fig. 4f). Under illumination, these unoccupied states can be activated as recombination centers. With the increase of light intensity, more and more unoccupied states will be involved as recombination centers until E_{Fn} reached the conduction band, which hence increases the responsivity ("−50 V" line in Fig. 4c) [7]. When the light intensity is further increasing, the situation is similar with the one which V_g is close to V_{th}, and the responsivity decreases with the increase of laser intensity. For the pristine MoS_2 device, there appear few recombination centers due to the existence of deep traps, and there is no increase part of the responsivity ("−50 V" line in Fig. 4d).

The vdW passivation has great impact on the response dynamics of the MoS_2 device as well. From the time-dependent photoresponse results depicted in Fig. 5, a clear improvement of both rise and decay response times of the MoS_2 device is observed after passivation. By defining the rise (decay) time as the duration when the drain current changes from 10% to 90% (90% to 10%) of its maximum value, we can compare the response dynamics between the

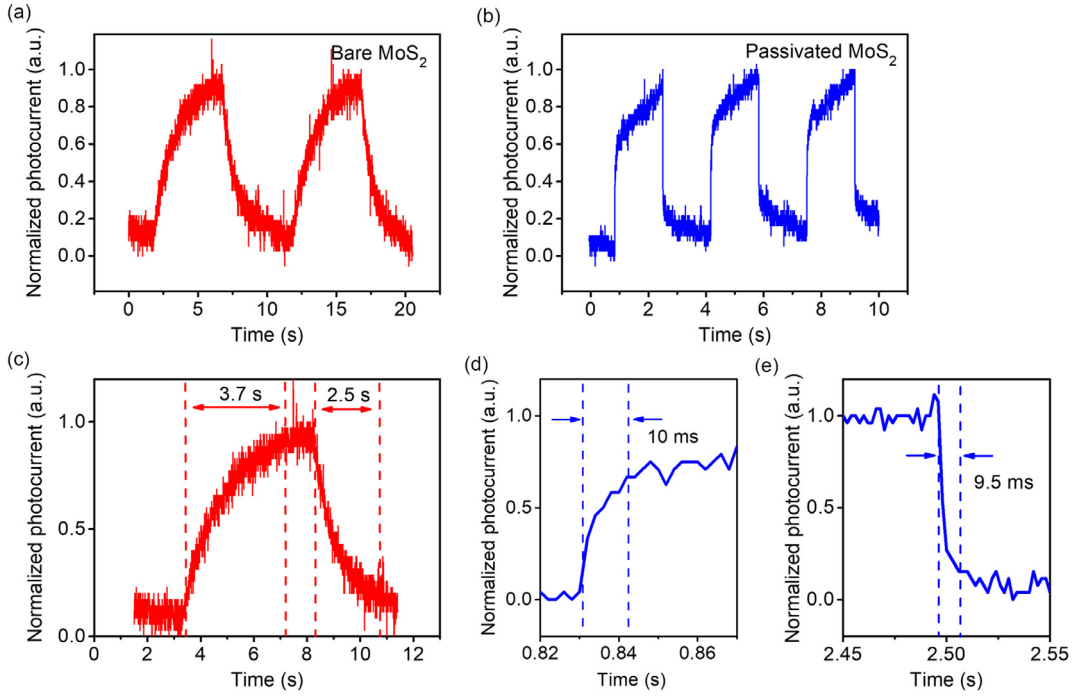

Fig. 5. (Color online) The photoresponse dynamics of monolayer MoS_2 (a) before and (b) after PTCDI-C13 passivation (V_g = 0 V, V_{ds} = 1 V, 650 nm illumination with 1 mW/cm^2 power density). (c) Details of rise and decay response times of bare monolayer MoS_2 device. (d), (e) Details of rise and decay response times of passivated MoS_2 device.

Table 2
Comparison of the device optoelectronic attributes before/after passivation.

Device structure	Responsivity (A/W)	Rising time	Decay time	Ref.
PTCDI-C13/MoS_2 (epitaxial growth)	1029/161	3.7 s/10 ms	2.5 s/9.5 ms	This work
ZnPc/MoS_2 (solution)	281/1.74	78 s/72 ms	25 s/8 ms	[29]
HfO_2/MoS_2 (ALD)	10^4/10	10 s/10 ms	NA	[7]

pristine and passivated devices. While the bare monolayer MoS_2 devices possessed an ultra-slow response time (rise edge of 3.5 s and decay edge of 2.5 s, Fig. 5c) which is dominated by the deep trap states, the response dynamics of the passivated device becomes faster by about three orders of magnitude (Fig. 5b). Fig. 5d, e shows the detailed response dynamics of the rising and decay edges, respectively (rising time of ~10 ms and decay time of ~9.5 ms). The fast response time mainly results from the reduction of the deep trap states presented in the pristine MoS_2. We have compared the detailed figures of merit of the passivated MoS_2 photodetector with other reported TMD devices using various passivation techniques (Table 2), illustrating the promising speed improvement by the vdW organic passivation. Importantly, while most of other passivation methods lead to the degradation of photoresponsivity by 2–3 orders of magnitude, our demonstrated PTCDI-C13 passivation induces limited decrease of photoresponsivity (from 1029 to 161 A/W). Further improvement of the optoelectronic properties is expected via excitonic engineering [52].

4. Conclusion

We have demonstrated a new passivation method with 1L PTCDI-C13 molecule on monolayer MoS_2 surface. The devices after passivation become much more stable in ambient and the hysteresis loops are largely eliminated. The MoS_2 FETs show significant improvement after passivation in terms of both carrier mobility and *SS*, due to the elimination of defects and isolation of ambient. Also, the photoresponse speed after passivation becomes much faster (response time ~10 ms). Our method provides a promising approach of fabricating high-performance 2D TMD based devices for various applications.

Conflict of interest

The authors declare that they have no conflict of interest.

Acknowledgment

The work was in part supported by Research Grants Council of Hong Kong SAR (AoE/P-03/08, AoE/P-02/12, 14204616, N_CUHK438/18), CUHK Group Research Scheme, CUHK Impact Postdoctoral Fellowship, and Innovation and Technology Commission, Hong Kong SAR Government (ITS/390/18).

Author contributions

Xin Xu, Li Tao, Zefeng Chen and Beilei Sun carried out the experiments. Li Tao and Jian-Bin Xu directed the project. All authors analyzed and discussed the data. Xin Xu, Li Tao and Jian-Bin Xu wrote the paper with input from all authors.

Appendix A. Supplementary materials

Supplementary materials to this article can be found online at https://doi.org/10.1016/j.scib.2019.09.009.

References

[1] Mak KF, Shan J. Photonics and optoelectronics of 2D semiconductor transition metal dichalcogenides. Nat Photon 2016;10:216–26.
[2] Li X, Tao L, Chen Z, et al. Graphene and related two-dimensional materials: structure-property relationships for electronics and optoelectronics. Appl Phys Rev 2017;4:021306.
[3] Liu P, Xiang B. 2D hetero-structures based on transition metal dichalcogenides: fabrication, properties and applications. Sci Bull 2017;62:1148–61.
[4] Cai Z, Liu B, Zou X, et al. Chemical vapor deposition growth and applications of two-dimensional materials and their heterostructures. Chem Rev 2018;118:6091–133.
[5] Tao L, Chen K, Chen Z, et al. Centimeter-scale CVD growth of highly crystalline single-layer MoS_2 film with spatial homogeneity and the visualization of grain boundaries. ACS Appl Mater Interfaces 2017;9:12073–81.
[6] Lopez-Sanchez O, Lembke D, Kayci M, et al. Ultrasensitive photodetectors based on monolayer MoS_2. Nat Nanotechnol 2013;8:497–501.
[7] Kufer D, Konstantatos G. Highly sensitive, encapsulated MoS_2 photodetector with gate controllable gain and speed. Nano Lett 2015;15:7307–13.
[8] Radisavljevic B, Radenovic A, Brivio J, et al. Single-Layer MoS_2 transistors. Nat Nanotechnol 2011;6:147–50.
[9] Liu H, Ye PD. MoS_2 dual-gate MOSFET with atomic-layer-deposited Al_2O_3 as top-gate dielectric. IEEE Electron Device Lett 2012;33:546–8.
[10] Liu D, Guo Y, Fang L, et al. Sulfur vacancies in monolayer MoS_2 and its electrical contacts. Appl Phys Lett 2013;103:183113.
[11] Santoch KC, Longo RC, Addou R, et al. Impact of intrinsic atomic defects on the electronic structure of MoS_2 monolayers. Nanotechnology 2014;25:375703.
[12] Park JH, Sanne A, Guo Y, et al. Defect passivation of transition metal dichalcogenides via a charge transfer van der Waals interface. Sci Adv 2017;3:e1701661.
[13] Wu H, Liu Y, Deng Z, et al. A field-effect approach to directly profiling the localized states in monolayer MoS_2. Sci Bull 2019;64:1049–55.
[14] Furchi MM, Polyushkin DK, Pospischil A, et al. Mechanisms of photoconductivity in atomically thin MoS_2. Nano Lett 2014;14:6165–70.
[15] Di Bartolomeo A, Genovese L, Foller T, et al. Electrical transport and persistent photoconductivity in monolayer MoS_2 phototransistors. Nanotechnology 2017;28:214002.
[16] Di Bartolomeo A, Genovese L, Giubileo F, et al. Hysteresis in the transfer characteristics of MoS_2 transistors. 2D Mater 2017;5:015014.
[17] Tongay S, Zhou J, Ataca C, et al. Broad-range modulation of light emission in two-dimensional semiconductors by molecular physisorption gating. Nano Lett 2013;13:2831–6.
[18] Cheng L, Qin X, Lucero AT, et al. Atomic layer deposition of a high-k dielectric on MoS_2 using trimethylaluminum and ozone. ACS Appl Mater Interfaces 2014;6:11834–8.
[19] Kayyalha M, Chen YP. Observation of reduced 1/f noise in graphene field effect transistors on boron nitride substrates. Appl Phys Lett 2015;107:113101.
[20] Tao L, Chen Z, Li X, et al. Hybrid graphene tunneling photoconductor with interface engineering towards fast photoresponse and high responsivity. npj 2D Mater Appl 2017;1:19.
[21] Tao L, Li H, Sun M, et al. Enhanced photoresponse in interfacial gated graphene phototransistor with ultrathin Al_2O_3 dielectric. IEEE Electron Device Lett 2018;39:987–90.
[22] Park W, Park J, Jang J, et al. Oxygen environmental and passivation effects on molybdenum disulfide field effect transistors. Nanotechnology 2013;24:095202.
[23] Das S, Chen H-Y, Penumatcha AV, et al. High performance multilayer MoS_2 transistors with scandium contacts. Nano Lett 2013;13:100–5.
[24] Na J, Joo MK, Shin M, et al. Low-frequency noise in multilayer MoS_2 field-effect transistors: the effect of high-k passivation. Nanoscale 2014;6:433–41.
[25] Lee G-H, Cui X, Kim YD, et al. Highly stable, dual-gated MoS_2 transistors encapsulated by hexagonal boron nitride with gate-controllable contact, resistance, and threshold voltage. ACS Nano 2015;9:7019–26.
[26] Li C, Yan X, Bao W, et al. Low sub-threshold swing realization with contacts of graphene/h-BN/MoS_2 heterostructures in MoS_2 transistors. Appl Phys Lett 2017;111:193502.
[27] Li H, Li X, Park J-H, et al. Restoring the photovoltaic effect in graphene-based van der Waals heterojunctions towards self-powered high-detectivity photodetectors. Nano Energy 2019;57:214–21.
[28] Jiang J, Ling C, Xu T, et al. Defect engineering for modulating the trap states in 2D photoconductors. Adv Mater 2018;30:1804332.
[29] Huang Y, Zhuge F, Hou J, et al. Van Der Waals coupled organic molecules with monolayer MoS_2 for fast response photodetectors with gate-tunable responsivity. ACS Nano 2018;12:4062–73.

[30] Meng Y, Ling C, Xin R, et al. Repairing atomic vacancies in single-layer $MoSe_2$ field-effect transistor and its defect dynamics. npj Quantum Mater 2017;2:16.
[31] Artel V, Guo Q, Cohen H, et al. Protective molecular passivation of black phosphorus. npj 2D Mater Appl 2017;1:6.
[32] Pak J, Min M, Cho K, et al. Improved photoswitching response times of MoS_2 field-effect transistors by stacking p-type copper phthalocyanine layer. Appl Phys Lett 2016;109:183502.
[33] Wang H, Xiao Y, Chen Z, et al. Solution-processed PCDTBT capped low-voltage $InGaZnO_x$ thin film phototransistors for visible-light detection. Appl Phys Lett 2015;106:242102.
[34] Thi QH, Kim H, Zhao J, et al. Coating two-dimensional MoS_2 with polymer creates a corrosive non-uniform interface. npj 2D Mater Appl 2018;2:34.
[35] He J, Yang Y, He Y, et al. Low noise and fast photoresponse of few-layered MoS_2 passivated by MA_3Bi_2Br 9. ACS Photon 2018;5:1877–84.
[36] Qian J, Jiang S, Li S, et al. Solution-processed 2D molecular crystals: fabrication techniques, transistor applications, and physics. Adv Mater Technol 2019;4:1800182.
[37] Tao L, Li H, Gao Y, et al. Deterministic and etching-free transfer of large-scale 2D layered materials for constructing interlayer coupled van der Waals heterostructures. Adv Mater Technol 2018;3:1700282.
[38] Jang J, Nam S, Chung DS, et al. High T_g cyclic olefin copolymer gate dielectrics for *N*, N′-ditridecyl perylene diimide based field-effect transistors: improving performance and stability with thermal treatment. Adv Funct Mater 2010;20:2611–8.
[39] Zhang Y, Qiao J, Gao S, et al. Probing carrier transport and structure-property relationship of highly ordered organic semiconductors at the two-dimensional limit. Phys Rev Lett 2016;116:016602.
[40] Kropp JA, Cai Y, Yao Z, et al. Atomic layer deposition of Al_2O_3 and TiO_2 on MoS_2 surfaces. J Vac Sci Technol A 2018;36:06A101.
[41] Lee Y-H, Zhang X-Q, Zhang W, et al. Synthesis of large-area MoS_2 atomic layers with chemical vapor deposition. Adv Mater 2012;24:2320–5.
[42] Koopman WA, Natali M, Donati GP, et al. Charge-exciton interaction rate in organic field-effect transistors by means of transient photoluminescence electromodulated Spectroscopy. ACS Photon 2017;4:282–91.
[43] Gündüz B, Kurban M. Photonic, spectroscopic properties and electronic structure of PTCDI-C8 organic nanostructure. Vib Spectrosc 2018;96:46–51.
[44] Tatemichi S, Ichikawa M, Koyama T, et al. High mobility n-type thin-film transistors based on *N*, *N*′-ditridecyl perylene diimide with thermal treatments. Appl Phys Lett 2006;89:112108.
[45] Roh J, Lee J, Kang C, et al. Air stability of PTCDI-C13-based n-OFETs on polymer interfacial layers. Phys Status Solidi Rapid Res Lett 2013;7:469–72.
[46] Late DJ, Liu B, Matte HSSR, et al. Hysteresis in single-layer MoS_2 field effect transistors. ACS Nano 2012;6:5635–41.
[47] Di Bartolomeo A, Grillo A, Urban F, et al. Asymmetric Schottky contacts in bilayer MoS_2 field effect transistors. Adv Funct Mater 2018;28:1800657.
[48] Alharbi A, Huang Z, Taniguchi T, et al. Effect of substrate coupling on the performance and variability of monolayer MoS_2 transistors. IEEE Electron Device Lett 2019;40:135–8.
[49] Gao J, Li B, Tan J, et al. Aging of transition metal dichalcogenide monolayers. ACS Nano 2016;10:2628–35.
[50] Chen X, Shinde SM, Dhakal KP, et al. Degradation behaviors and mechanisms of MoS_2 crystals relevant to bioabsorbable electronics. NPG Asia Mater 2018;10:810–20.
[51] Streetman BG. Carrier recombination and trapping effects in transient photoconductive decay measurements. J Appl Phys 1966;37:3137–44.
[52] Lien D-H, Uddin SZ, Yeh M, et al. Electrical suppression of all nonradiative recombination pathways in monolayer semiconductors. Science 2019;364:468–71.

Xin Xu received his B.S. degree in Physics from Nanjing University in 2016. Now, he is a Ph.D. student of Electronic Engineering in The Chinese University of Hong Kong supervised by Prof. Jian-Bin Xu. His research mainly focuses on electrical and optical properties of two-dimensional materials and organic materials.

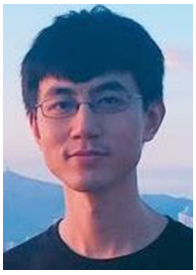

Li Tao is currently a Postdoctoral Fellow in the Department of Electronic Engineering, The Chinese University of Hong Kong. He obtained his Ph.D. degree in Electronic Engineering in 2018 from the same department supervised by Prof. Jian-Bin Xu. Prior to that, he received B.S. and M.S. degrees in Physics from Hunan University and National Center for Nanoscience and Technology (NCNST, CAS), respectively. His research interests include the growth, electronic/optoelectronic devices and light-matter interactions of two-dimensional materials.

Jian-Bin Xu has been Professor of Department of Electronic Engineering, since 2002; Director of Materials Science and Technology Research Center in The Chinese University of Hong Kong (CUHK) since 2007, and is Vice-Chancellor's Outstanding Fellow of the Faculty of Engineering and Chang Jiang (Cheung Kong) Scholar Chair Professor by Ministry of Education of China. He received his B.Sc. and M.Sc. degrees from Nanjing University in 1983 and 1986, respectively, in Physics and Information Physics. Since 1988, he was privileged to pursue his Ph.D. study in the University of Konstanz (an elite university), where he earned his doctorate (Dr. rer. nat.) in 1993. Afterwards, he has been with the Department of Electronic Engineering, CUHK. His research interests currently include perovskite optoelectronics, organic semiconductors, two-dimensional layered materials, functional oxide materials, etc.